Effect of an applied magnetic field on the relaxation time of single-chain magnets

Claude Coulon,[1] Rodolphe Clérac,[1] Wolfgang Wernsdorfer,[2] Thierry Colin,[3] Ayumi Saitoh,[4] Natsuko Motokawa,[4] and Hitoshi Miyasaka[4]

[1]*Université Bordeaux 1, CNRS, Centre de Recherche Paul Pascal, UPR-CNRS 8641, 115 Avenue Dr. A. Schweitzer, 33600 Pessac, France*

[2]*Institut Néel, Associé à l'UJF, CNRS, Boîte Postale 166, 38042, Grenoble Cedex 9, France*

[3]*Université Bordeaux 1, INRIA Futurs, Projet MC2, IMB, 351 Cours de la Libération, 33400 Talence, France*

[4]*Department of Chemistry, Graduate School of Science, Tohoku University, 6-3 Aramaki-Aza-Aoba, Aoba-ku, Sendai, Miyagi 980-8578, Japan*

(Received 27 July 2007; revised manuscript received 16 October 2007; published 21 December 2007)

Single-chain magnets (SCMs) are one-dimensional systems in which the relaxation of the magnetization becomes very slow at low temperature. This singular behavior is due to the vicinity of the critical point located at vanishing temperature ($T=0$) and applied magnetic field ($H=0$). In order to optimize the properties of these nano-objects, detailed studies of the observed critical behavior are necessary. However, previous works on the SCM relaxation have essentially analyzed experimental data in the absence of applied magnetic field. We discuss in this paper the effect of applying a magnetic field on two different examples of single-chain magnets. These samples have been previously described in the absence of magnetic field and considered as model systems since their chains are composed of a regular one-dimensional (1D) arrangement of anisotropic trimer units. These magnetic trinuclear motifs can be described at low temperature as effective spins coupled ferromagnetically. Theoretical results relevant to analyze our data in the presence of an applied magnetic field are first described. We also present a simple numerical approach to discuss finite-size effects relevant in SCM systems. Experimental data, including ac and dc data on powder samples and single crystals, are then presented. These results are analyzed and compared with the theoretical predictions deduced for the 1D Ising model. At low field, for $h\xi \ll 1$ (where ξ is the correlation length normalized to the unit cell parameter and $h=\mu H/k_B T$ is the dimensionless applied field) or for $hL \ll 1$ when finite-size effects are relevant (L being the chain length normalized to the unit cell parameter), we show that experimental data reproduce the critical behavior expected from the theory. Moreover, the obtained values of ξ or L are in excellent agreement with the estimation deduced from susceptibility data. At higher fields, for $h\xi \gg 1$ or $hL \gg 1$, we show that the field dependence of the relaxation time is drastically different for the two samples. This difference is understood taking into account the field dependence of the relaxation time of the effective spins located inside a domain wall.

DOI: 10.1103/PhysRevB.76.214422 PACS number(s): 75.10.Pq, 75.40.Gb, 75.50.Xx, 75.75.+a

I. INTRODUCTION

The search for new magnetic nanomaterials suitable for information storage is presently a very active field of research. Among others, single-chain magnets (SCMs) have been recently described. Although the first experimental report of such systems is quite recent,[1] the number of SCM compounds and their experimental studies are rapidly increasing.[2] SCM materials are essentially composed of magnetically isolated chains. At thermal equilibrium, the resulting one-dimensional system remains in a paramagnetic phase at any finite temperature but can be prepared at low temperature in a metastable state with a finite magnetization in the absence of any applied magnetic field. The reason for this striking behavior is the coexistence of strong uniaxial anisotropy and intrachain magnetic correlations. In this case, the characteristic time for the relaxation of the magnetization becomes very long at low temperatures. A finite magnetization can then be frozen in the absence of magnetic field and the material can be considered as a *magnet*.

For a theoretical understanding of the SCM behavior, the simplest case is a chain composed of a regular arrangement of identical ferromagnetically coupled magnetic units. The low temperature increase of the relaxation time can then be discussed as a *critical slowing down* resulting from the vicinity of the ferromagnetic critical point located for this one-dimensional system at $T=0$ and $H=0$ (i.e., at vanishing temperature and applied magnetic field). While a divergence of the relaxation time is expected for any order parameter dimensionality, the largest effect is obtained for "Ising-like" systems with an easy magnetic axis. In fact, in this case, the magnetic correlations are the most developed between magnetic units at a given temperature and for a given strength of the magnetic interaction as the correlation length ξ varies exponentially at low temperature for an infinite chain.[2] Although some theoretical analysis of more complex chains is still possible, it is important to analyze experimental results on simple SCMs for a detailed comparison with the theory. This confrontation is certainly a crucial step for further improvements of these materials, in particular, for future applications to information storage.

In this paper, we will describe two examples of such SCM systems in which the chains can be described as a regular arrangement of $[Mn^{III}\text{-}Fe^{III}\text{-}Mn^{III}]$ and $[Mn^{III}\text{-}Ni^{II}\text{-}Mn^{III}]$ trinuclear units, respectively.[3–5] In these chains, dominant antiferromagnetic interactions are found inside the trimers, i.e.,

between Mn and Fe or Ni atoms, while weaker ferromagnetic couplings exist between Mn atoms. Then, the trimer motifs can be magnetically described at low temperatures as single effective spins ($S=9/2$ and $S=3$, respectively) coupled ferromagnetically. The chains are then described as a regular array of these magnetic units. Moreover, the presence of single ion anisotropy brought by the Mn(III) metal ions implies that each trinuclear motif is an anisotropic unit exhibiting an easy axis pointing in a unique direction along the chain.[3–5] Therefore, these examples of single-chain magnets can be considered as model systems for a detailed analysis of the magnetic relaxation.

As far as we know, magnetic relaxation of SCMs has only been studied at nonzero field via the field sweep rate and temperature dependence of the coercive field.[6] The data were analyzed with a model of thermally activated nucleation of magnetization reversal. Below 1 K, the coercive field became temperature independent but remained strongly sweep rate dependent. In this temperature range, it was proposed that the reversal of the magnetization is induced by a quantum nucleation of a domain wall that then propagates due to the applied field. However, the effect of an applied magnetic field on the critical behavior has not been considered yet and is the topic of this report. The organization of the paper will be as follows: (i) The theoretical background relevant for the analysis of the experimental results will be presented in Sec. II, including a numerical study to discuss finite-size effects expected to be relevant in a real sample at low temperature. (ii) Experimental results will be presented in Sec. III. (iii) Their analysis in relation with Sec. II will then be given in Sec. IV. Finally, (iv) Sec. V will present our concluding remarks.

II. THEORETICAL BACKGROUND

A. Thermodynamic properties

As mentioned in the previous section, the SCM systems studied in this paper are composed of trinuclear units that can be described as single anisotropic magnetic motifs at low temperature. Quite generally, the anisotropy energy is finite and should be compared with the exchange coupling between neighboring magnetic units. Introducing single ion anisotropy, a realistic Hamiltonian to describe a chain is the anisotropic Heisenberg model:

$$H = -2J\sum_{-\infty}^{+\infty} \vec{S}_p \vec{S}_{p+1} + D\sum_{-\infty}^{+\infty} S_{pz}^2, \tag{1}$$

where J and D are, respectively, the exchange and anisotropy energies. Taking $\mathbf{z}$ as the easy axis, D is negative (we will only consider this case in the following). In Eq. (1), each magnetic motif composing the chains is described as an effective spin of size S. Ferromagnetic couplings between these units imply that J is a positive energy. In the large anisotropy limit ($|D| \gg J$), the anisotropic Heisenberg model can be reduced to the Ising Hamiltonian:

$$H = -J_I\sum_{-\infty}^{+\infty} \sigma_p \sigma_{p+1}, \tag{2}$$

where $J_I=2JS^2$ is the effective Ising exchange interaction and $\sigma_p=\pm 1$ describes the orientation of the pth magnetic unit of the chain.

Exact thermodynamic results are available in one dimension for Hamiltonians (1) and (2).[7] In both cases, the low temperature magnetic ground state can be described as large oriented domains of average size 2ξ (where ξ is the correlation length) separated by narrow domain walls. ξ increases exponentially for an infinite chain with an activation energy equal to the creation energy of a domain wall. When the anisotropy energy is large enough ($|D|/J>4/3$), narrow domain walls are obtained and the activation energy of ξ becomes $2J_I$.[2] The two SCM systems described experimentally in this paper are expected to be in this limit.[3–5] Note that this activation energy is readily obtained when plotting χT versus $1/T$ (where χ is the spin susceptibility) as this quantity is proportional to the correlation length.[2,7]

To conclude this short paragraph, it is useful to mention that thermodynamic properties of a finite Ising chain have also been described.[8] As expected, χT saturates when the chain length becomes of the order of ξ, i.e., when the growth of the magnetic correlations is limited by finite-size effects.

B. Dynamic properties at $H=0$

The study of the dynamic properties has been essentially developed using the Ising model. In the one-dimensional case, the pioneering work to investigate the dynamics is due to Glauber.[9] The Glauber model is a stochastic description of the dynamics assuming that the transition probability for a given spin only depends on the local field experienced by this spin. More precisely, the Glauber choice for the transition probability of a given spin σ_p is

$$\omega_{p0}(\sigma_p) = \frac{1}{2\tau_0}\left(1 - \frac{\gamma}{2}\sigma_p(\sigma_{p-1} + \sigma_{p+1})\right), \tag{3}$$

where $\gamma=\tanh(2J_I/k_BT)$ (k_B is the Boltzmann constant and T is the temperature) and τ_0 is the characteristic time for a spin flip in the absence of internal field (called $1/\alpha$ in Ref. 9). In SCMs, one expects τ_0 to be activated with an activation energy related to the anisotropy barrier experienced by each spin unit composing the chain.[4] With this assumption, an exact solution can be obtained in the one-dimensional case in the absence of applied magnetic field. The main result is a divergence of the relaxation time as

$$\tau(T) = 2\tau_0\xi^2, \tag{4}$$

where ξ is the correlation length normalized to the unit cell parameter. This simple result essentially relies on random motion of the domain walls[10] and should also be valid for large but finite anisotropy. In the Ising limit and at low temperature, ξ is equal to $e^{2K}/2$, where $K=J_I/k_BT$.[11] For the same reason, Eq. (4) is not specific to the Glauber model and other expressions of the transition probability give the same dynamical critical exponent.[12] This argument will be further developed in the next section.

Although most of the theoretical studies have been devoted to infinite chains, finite-size effects have been described in real SCM systems.[4,13] In fact, a small number of defects are always present in real materials. As the temperature decreases, the correlation length of the infinite chain that increases exponentially becomes larger than the mean distance between two defects. A crossover temperature is then reached, and finite-size effects become relevant at lower temperatures. In this case, the conclusions of the Glauber model for the infinite chain are no longer valid. In this limit, the chain should be divided into finite segments and the simplest description is obtained assuming that all the segments have the same size L. The relaxation of such a segment for $H=0$ has been previously described in the literature.[14,15] Far below the crossover temperature, the scaling of the relaxation time becomes

$$\tau(T) = \tau_0 \xi L, \tag{5}$$

where both ξ and L are normalized to the unit cell parameter. An equivalent expression in the Ising limit and at low temperature is $\tau(T)=\tau_0 L e^{2K}/2$.

C. Dynamic properties at $H \neq 0$

Describing the dynamics of an Ising chain under a magnetic field is more complex. The Glauber assumption for the transition probability becomes

$$\omega_p(\sigma_p) = \omega_{p0}(\sigma_p)(1 - C\sigma_p), \tag{6}$$

where $\omega_{p0}(\sigma_p)$ is given by Eq. (3) and $C=\tanh(\mu H/k_B T)$ (μ is the magnetic moment of each magnetic unit).

When $H \neq 0$, this model has never been exactly solved even for a chain. However, several publications have discussed the effect of an applied magnetic field on the Ising chain dynamics. Many of them are dedicated to biopolymers and to the description of the helix-coil transition.[16–23] In fact, a simplified description of this transition relies on a two-state model where a macromolecule of N segments is built with either helix (equivalent to $\sigma_i=+1$) or coil (equivalent to $\sigma_i=-1$) units. The two parameters introduced to describe the equilibrium properties are called σ and s. The correspondences with the Ising model are $\sigma=e^{-4K}$ and $s=e^{2h}$, where h is the dimensionless field parameter: $h=\mu H/k_B T$. The dynamics is, in the most general case, controlled by three kinetic parameters as illustrated in Fig. 1. First, k_F is the rate constant for the growth of a helix domain (or a spin up domain in the Ising description). The rate constant of the inverse process should be k_F/s to satisfy the detailed balance condition. Second, there are two other kinetic parameters, γ_C and γ_H, associated with the coil and helix nucleations. Again, the detailed balance condition imposes the rate constants of the inverse processes (see Fig. 1).

In the frame of the Glauber model [considering Eq. (6)], there is only one kinetic parameter, i.e., $k_F(h=0)$, that we called $1/\tau_0$ in our previous publications.[2–6] Using Eq. (6), one deduces[23,24]

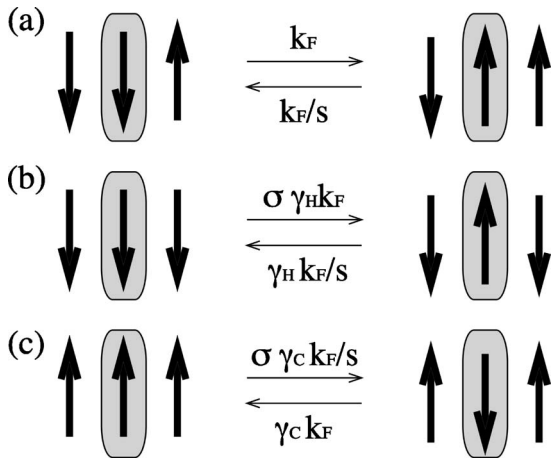

FIG. 1. Definition of the different kinetic constants for the dynamic equations: (a) cluster growth and (b), (c) cluster nucleation.

$$k_F = \frac{1}{\tau_0}\frac{s}{s+1}, \quad \gamma_H = \frac{s+1}{s\sigma+1}, \quad \gamma_C = \frac{s+1}{s+\sigma}. \tag{7}$$

However, different field dependences of these parameters are also possible. The only condition required to preserve the symmetry of the problem is $\tau(h)=\tau(-h)$. This implies

$$k_F(s) = s k_F(1/s) \quad \text{and} \quad \gamma_C(s) = \gamma_H(1/s). \tag{8}$$

The dynamics can then be formulated in terms of kinetic equations for cluster concentrations. Quite generally, one expects a "polydisperse" (i.e., a "multitime") relaxation, and the dynamic response of the system is therefore complex. However, the essential information on the relaxation is captured with the so-called initial relaxation time, which can be explicitly obtained for a linear response of the system. The result for the infinite chain is

$$\frac{1}{\tau} = k_F \frac{(s-1)^2 + 4\sigma s}{s\lambda_0}\left(1 + (\gamma_H - 1)\frac{\lambda_0 - s}{(1+s)\lambda_0} + (\gamma_C - 1)\frac{s(\lambda_0 - 1)}{(1+s)\lambda_0}\right), \tag{9}$$

where $\lambda_0=(s+1+\sqrt{(s-1)^2+4\sigma s})/2$.

The result for the Glauber model is readily obtained introducing the expressions of the kinetic coefficients given by Eq. (7).[25] The general result given by Eq. (9) can be simplified at low field when $he^{2K} \ll 1$ to describe the critical regime. In this case, the last term of Eq. (9) becomes negligible, and a simplified expression of the relaxation time is

$$\frac{1}{\tau} \approx 2k_F(h^2 + \sigma). \tag{10}$$

As expected for a ferromagnetic critical point, h has a strong effect on the critical behavior and the relaxation time rapidly decreases with h at a given temperature. A universal result is then obtained for the infinite chain in the critical regime (neglecting the field dependence of k_F):

$$\tau(h) = \frac{\tau(h=0)}{1 + e^{4K} h^2}. \tag{11}$$

The same expression has also been deduced from other theoretical studies.[26–29]

The nonlinear response has also been investigated and compared with the linear case.[18,23,24] Strictly speaking, the linear and nonlinear results are different, and this difference is the largest for intermediate values of s.[23] The local-equilibrium approximation described in the next section gives a simple opportunity to estimate this difference. The linear response is easily obtained (see Appendix A), and the nonlinear solution can be explicitly written for any initial conditions.[27] Starting, for example, with a saturated magnetization at $t=0$, we have checked that the nonlinear response can be reasonably approximated to a single exponential signal for small values of $\sigma=\exp(-4K)$, while the deduced relaxation time was close to the one obtained for the linear response.[30] Therefore, our experimental results will be essentially compared with the theoretical linear response for which explicit and compact results are available.

Finite-size effects have also been previously discussed in the literature.[19,21,22,29,31] In this regime, the critical behavior is expected to be blunt. The most explicit expression of the relaxation time of a finite chain is found in Ref. 19 considering the linear response in the case $\gamma_C=\gamma_H=1$. The kinetic coefficients, giving the transition probabilities of Ref. 15 at the chain ends, correspond to $\beta=\beta'=1$ [see Eq. (43) of Ref. 19]. The scaling law at $H=0$ [i.e., Eq. (5)] is obtained (see Fig. 6 of Ref. 19) and a complex expression of the relaxation time for $H\neq 0$ is also given. However, this expression can be simplified at low temperature (when $\sigma\to 0$) and for small values of h (typically for $Lh<3$) as

$$\frac{\tau(h=0)}{\tau(h)} \approx \frac{\tanh(Lh)}{Lh(1-\tanh^2(Lh))}. \tag{12}$$

This result shows that Lh becomes the relevant reduced variable. Moreover, in the critical regime ($Lh \ll 1$), the approximate low temperature expression becomes

$$\tau(h) = \frac{\tau(h=0)}{1 + 2L^2h^2/3}. \tag{13}$$

D. Numerical study of the finite chain

Although theoretical expressions of the relaxation time for $H\neq 0$ are available even for finite chains, we have developed a complementary numerical treatment of the dynamics. Several reasons and limitations of the available theoretical expressions have initiated this approach. First, as far as we know, a general and compact expression of the relaxation time using the Glauber coefficients [Eq. (7)] is not available. Second, in the available theoretical approaches, the kinetics of the transition is described in terms of dynamic cluster concentrations rather than in terms of time dependence of the spin values (as it was the case for $H=0$). Moreover, for a finite chain, the eigenmodes associated with the smallest eigenfrequencies cannot be easily obtained, and the relevance of a single-time approximation cannot be simply discussed. Overall, these limitations motivate us to develop a numerical treatment to this problem. To generalize the approach described in Refs. 9 and 15 for $H\neq 0$, some approximations are necessary. In fact, even using Eq. (6), Glauber has shown that the problem becomes more complex when a magnetic field is applied. In this case, the differential equations describing the dynamics of the average spins contain pair-correlation terms [see Eq. (85) of Ref. 9]. In the same way, the equations describing the dynamics of pair-correlation functions contain correlation functions of higher order and so on. This complex system of coupled differential equations has no simple solution but several approximations can be proposed to simplify the problem. Some of them have been already introduced for the infinite chain.[27] Among them, the "local-equilibrium" method assumes that the relation between the pair-correlation function and the magnetization is the same at any time as at thermal equilibrium. For the infinite chain, a single nonlinear differential equation is then sufficient to describe the dynamics of the magnetization. Remarkably, this nonlinear equation is exactly soluble and can be linearized to describe a small departure from equilibrium (the linear response of the system). We show in Appendix A that the resolution of this linear equation is straightforward. The obtained relaxation time describes correctly the critical regime [i.e., gives Eq. (11)] but also reproduces the solution of the Glauber model [Eq. (9) using the kinetic coefficients given by Eq. (7)] as long as the obtained relaxation time remains significantly larger than τ_0. As this condition is always valid to analyze experimental results, this approximation can be used to discuss the dynamics of the finite chain. Details of the calculation are given in Appendixes B and C. Indeed, the method described in Ref. 15 can be fully generalized in the presence of a magnetic field. After linearization, the set of equations is used to determine numerically the eigenfrequencies and the corresponding eigenmodes of the chain and to discuss the critical regime. These calculations have been performed using SCILAB, an open source platform for numerical computation.[32]

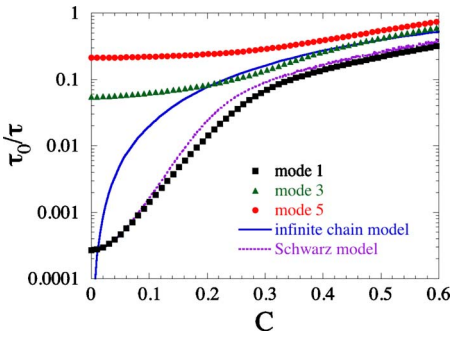

FIG. 2. (Color online) The eigenfrequencies (normalized to $1/\tau_0$) of three slowest symmetric modes (■, ▲, ●) as a function of C for $K=3$ and $L=20$. The continuous line gives the result for the initial time of the infinite chain. The dotted line gives the result for the finite chain ($K=3$ and $L=20$) using the simplified Schwarz model (Ref. 19).

Let us first comment on the results on the eigenfrequencies and eigenvectors. Quite generally, either symmetric or

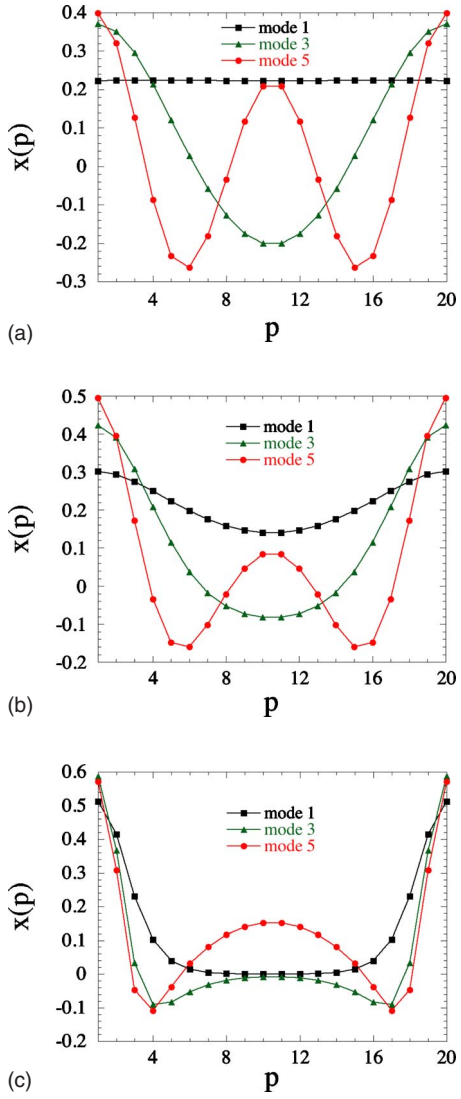

FIG. 3. (Color online) Components of the eigenvectors of three slowest symmetric modes for $K=3$ and $L=20$: (a) $C=0.1$, (b) $C=0.25$, and (c) $C=0.6$. The normalization is such as $\Sigma_{p=1}^{L} x_p^2=1$.

antisymmetric modes are found, for which $x(1)=\pm x(L)$, respectively, where $x(p)$ is the component for the site p $(1<p<L)$ of a normalized eigenvector. Only the symmetric modes that bear a magnetization will be considered in the following. An example of the three smallest eigenfrequencies for $K=3$ and $L=20$ is given in Fig. 2. The data above $C=0.6$ are not shown as the validity of the local-equilibrium approximation becomes questionable in this field regime (as τ_0/τ becomes too close to 1 even for the slowest modes). Two distinct field domains should be distinguished: (i) at low field $(C<0.3)$, the slowest mode has a frequency much smaller than the one of the other modes and, therefore, the single-time approximation should be valid; (ii) on the other hand, the difference between successive eigenfrequencies becomes smaller at higher fields. For a deeper discussion, the corresponding eigenvectors should be considered as shown in Fig. 3 for three selected values of the magnetic field. Figure 3(a) is representative of the case $C<0.3$ that is a situation reminiscent of the $h=0$ case where $x(p)\propto\cos[(p-(L+1)/2)\theta_i]$, with $\theta_i\approx(i-1)(2\pi/L)$ (i is the mode number).[15] When C increases, the slowest mode (mode 1) is more and more localized at the chain ends [see Fig. 3(c)], and at the same time, its weight decreases as illustrated by Fig. 4 (the weight of a given mode is defined by the quantity $\beta=\Sigma_{p=1}^{L} x_p$ as β is proportional to the magnetization carried by this mode, with each eigenvector being normalized: $\Sigma_{p=1}^{L} x_p^2=1$). Then, above $C=0.3$, the single-time approximation becomes questionable as several modes become equally important. Simultaneously, the obtained frequencies become closer to the one of the infinite chain result (continuous line in Fig. 2), suggesting that finite-size effects are more drastically expected at low field ($C<0.2$ in the case of Fig. 2). Finally, Fig. 2 also shows that the result of the Schwarz simplified model (dotted line) remains close to our numerical estimation below $C=0.6$. Therefore, kinetic parameters γ_C and γ_H obviously do not play a critical role at low field, in the regime where the experimental results will be described in the next section.

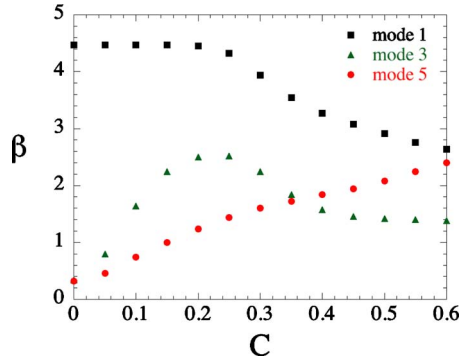

FIG. 4. (Color online) Weight of the different modes $\beta=\Sigma_{p=1}^{L} x_p$ for the three modes considered in Fig. 3 as a function of C.

Similar conclusions are obtained for other values of L and K as exemplified for $K=3$ and $L=100$ by Figs. 5 and 6 that give, respectively, for the modes bearing some magnetization the three smallest eigenfrequencies and the corresponding eigenvectors for two values of C. The weight of these three

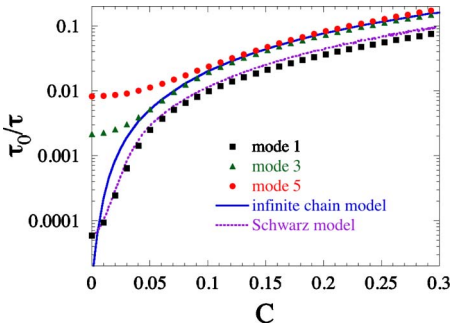

FIG. 5. (Color online) The eigenfrequencies (normalized to $1/\tau_0$) of the three slowest symmetric modes as a function of C for $K=3$ and $L=100$. The continuous line gives the result for the initial time of the infinite chain. The dotted line gives the result for the finite chain ($K=3$ and $L=100$) using the simplified Schwarz model (Ref. 19).

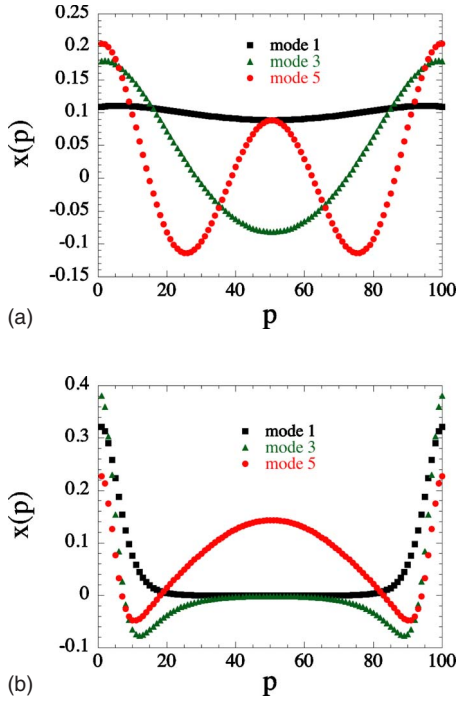

FIG. 6. (Color online) Components of the eigenvectors of three slowest symmetric modes for $K=3$ and $L=100$: (a) $C=0.03$ and (b) $C=0.2$. The normalization is the same as for Fig. 3.

slowest modes is also given in Fig. 7. In this case, the low field behavior is restricted to $C<0.04$. Again, the first mode becomes mostly localized at the chain ends at higher fields, while the next dominant modes have a frequency close to the one of the infinite chain. As for $L=20$, the result of the Schwarz model is close to the frequency of the slowest mode.

From this numerical approach, the critical regime ($he^{2K} \ll 1$ or $hL \ll 1$) can be described in detail. As the magnetic field is small in this domain, there is no need to distinguish between h and C. For these small field values, the frequency follows a quadratic h dependence, i.e., introducing the normalized frequency $\nu_{nor}(h)=\tau(h=0)/\tau(h)$, the low field expression of this normalized frequency reads $\nu_{nor}(h)=1+(a_i h)^2$. Figures 8 and 9 give the deduced value of a_i as a

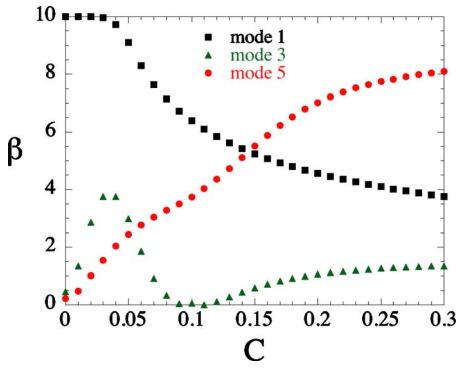

FIG. 7. (Color online) Weight of the three modes considered in Fig. 6 as a function of C.

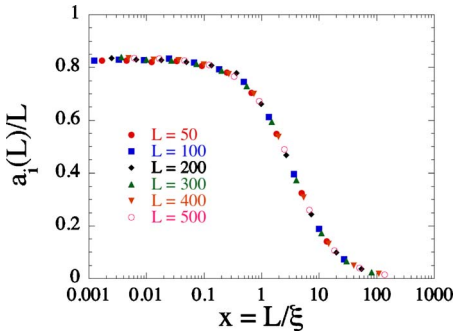

FIG. 8. (Color online) Numerical estimation of a_i normalized to the chain length as a function of $x=L/\xi$. This parameter is defined from the field dependence of the normalized frequency, $\nu_{nor}(h)=1+a_i^2h^2$, valid at low field.

function of the reduced variable $x=L/\xi$. When normalized to L (Fig. 8), a_i saturates to about $0.82L$ at low temperature, i.e., to a value consistent with $L\sqrt{2/3}$ as predicted by Eq. (13) deduced from the Schwarz model. A crossover is also observed when $x \approx 2$, i.e., when the size of the correlated domains (2ξ) equals the chain length (L). This crossover is also emphasized by Fig. 9, which shows a_i normalized to $2\xi=e^{2K}$. A master curve is found for the investigated values of the chain length: $a_i=2\xi f(x\sqrt{2/3})$, where the function f is the one introduced by Luscombe *et al.*[15] to describe the crossover for $H=0$: $\tau_L=\tau_\infty f(x)$, τ_L and τ_∞ being the relaxation time of the finite and infinite chains, respectively.[33] To summarize, the present numerical results give a simple description of the critical regime for a single-chain magnet at any temperature and chain length that will be used to analyze the experimental data in the next section.

III. EXPERIMENT

In the last few years, a large number of new materials have been reported as being single-chain magnets.[2] Most of them have a complex chain structure, and the comparison with simple theories is difficult. In fact, their magnetic behavior is, most of the time, simply characterized by dynamic susceptibility measurements to deduce the temperature de-

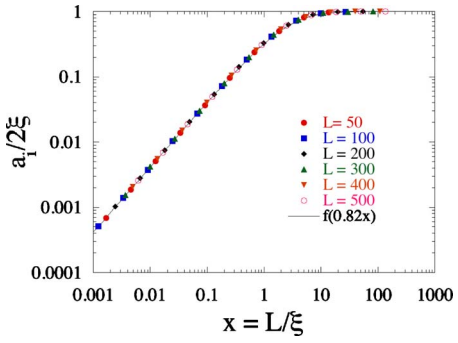

FIG. 9. (Color online) Numerical estimation of a_i normalized to $2\xi=e^{2K}$ as a function of $x=L/\xi$. The continuous curve is the function f introduced in Ref. 15 plotted as a function of $0.82x$.

pendence of the relaxation time for $H=0$. However, a series of materials has been published which presents a much simpler structure.[3–5] These chains present a regular ferromagnetic arrangement of trinuclear units that can be viewed as effective spins at low temperature. To study the effect of an applied magnetic field, we have chosen two of these systems. The first sample is $(NEt_4)[Mn_2(5\text{-}MeOsalen)_2Fe(CN)_6]$ abbreviated as the Mn/Fe chain in the following. In this system, the chain magnetic unit is a $[Mn^{III}\text{-}Fe^{III}\text{-}Mn^{III}]$ trimer that can be described as an effective $S=9/2$ spin at low temperature.[5] The second one is $[Mn_2(saltmen)_2Ni(pao)_2(py)_2](ClO_4)_2$ abbreviated as the Mn/Ni chain in the following, where the magnetic unit composing the chain is a $[Mn^{III}\text{-}Ni^{II}\text{-}Mn^{III}]$ trimer which can be described as an effective $S=3$ spin at low temperature.[3,4]

A. Summary of the magnetic properties at $H=0$

A detailed magnetic characterization of these two samples including a comparison of static and dynamic properties in the absence of applied magnetic field can be found in Refs. 3 and 5. Nevertheless, the most important results necessary to discuss the field effect are summarized briefly here. To emphasize the one-dimensional Ising-like behavior, the zero field susceptibility can be presented plotting $\ln(\chi T)$ versus $1/T$. A straight line is obtained at low temperature when the magnetic correlation length varies exponentially, i.e., when the effective spin approximation becomes valid. The normalization of χT to 1 when $1/T$ vanishes (i.e., at infinite temperature) leads to a quantity that will be called $\lambda(T)$ in the following. According to the theory, $\lambda(T)$ should be equal to e^{2K} in the exponential regime and to L below the crossover, when finite-size effects become relevant. Figure 10(a) gives $\lambda(T)$ versus $1/T$ for the Mn/Fe chain as deduced from the data of Ref. 5. An exponential regime is, in fact, observed experimentally, and the saturation at about 1.5 K has been described as the manifestation of finite-size effects. The slope in the exponential regime gives an estimation of the exchange energy, $J_1/k_B=3$ K, using the notation introduced in Sec. II. The temperature dependence of the relaxation time in the absence of applied magnetic field has also been reported. A semilogarithmic plot of $\tau(T)$ versus $1/T$ gives two linear regimes consistent with the theoretical predictions for the infinite chain and the finite-size regimes, respectively. The corresponding slopes are, respectively, equal to 31 and 25 K. These values are in quantitative agreement with Eqs. (4) and (5) if $J_1/k_B=3$ K (consistent with the susceptibility data) and $\Delta_a/k_B=19$ K, where Δ_a is the activation energy of τ_0.

Similar results have been found for the Mn/Ni chain. Figure 10(b) gives $\lambda(T)$ versus $1/T$ for the Mn/Ni chain as deduced from the data of Ref. 4. The slope in the exponential regime gives a larger value of the exchange energy, $J_1/k_B=14$ K, which explains that $\lambda(T)$ saturates at a much higher value, close to 80 in the present case. As in the previous case, the relaxation time exhibits two activated regimes, with corresponding slopes equal to 74 and 55 K, respectively. These two energy gaps are also in agreement with the former value of J_1, with $\Delta_a/k_B=23$ K.

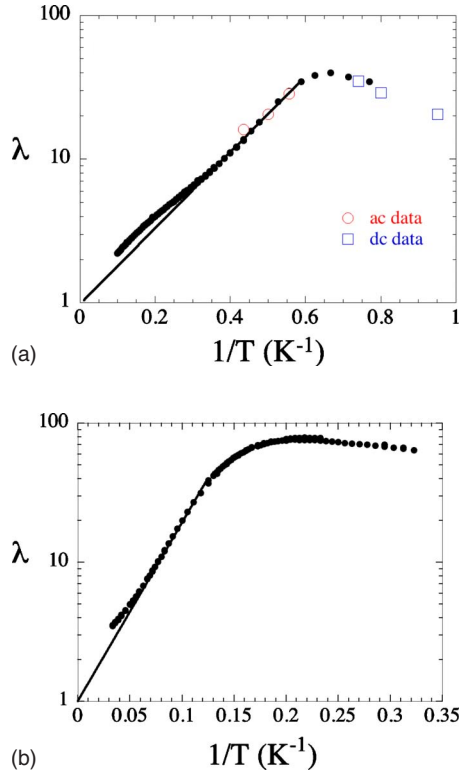

FIG. 10. (Color online) Semilogarithmic plot of $\lambda(T)$ (defined in the text) as a function of $1/T$ (full dots). (a) Mn/Fe chain. Open dots and open squares give the value deduced from the analysis given in Sec. IV, respectively, for ac and dc relaxation data. (b) Semilogarithmic plot of $\lambda(T)$ for the Mn/Ni chain.

To conclude this short presentation, it should be noted that in both systems, $\lambda(T)$ is not strictly constant below the crossover temperature but rather decreases slowly with temperature (see Fig. 10). This behavior has been imputed to a small departure from the ideal one-dimensional behavior of a finite chain, due, for example, to small interchain couplings.[4] This means that $\lambda(T)$ should be considered in the low temperature regime as a weakly temperature dependent effective chain length. This argument will be used in the following section to analyze the field dependence of the relaxation time of these systems.

B. Single-chain magnet behavior under magnetic field in the Mn/Fe chain

To deduce the relaxation time for different values of the applied magnetic field, ac susceptibility was first measured as a function of the frequency at a given temperature and field on a powder sample. The measurements have been performed using a Quantum Design superconducting quantum interference device (SQUID) magnetometer MPMS-XL with an oscillating ac field of 3 Oe and frequencies ranging from 1 to 1500 Hz. Figures 11(a) and 11(b) give, respectively, the real and imaginary parts of the ac susceptibility for selected values of the magnetic field at 1.8 K. The variation of characteristic frequency (i.e., of the inverse of the relaxation time) with the applied field is readily obtained taking the

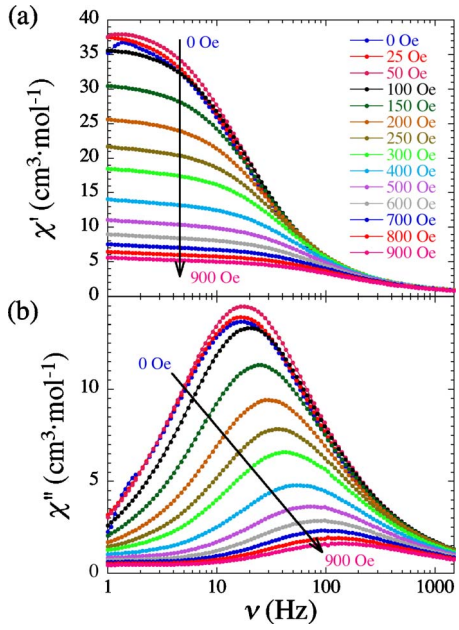

FIG. 11. (Color online) Real part (top) and imaginary part (bottom) of the ac susceptibility at 1.8 K of the Mn/Fe chain for selected values of the applied magnetic field.

maximum of the imaginary part of the susceptibility. From Fig. 11, it is clear that the characteristic frequency increases with the field strength. Figure 12 gives the field variation of the normalized frequency ν_{nor} at three different temperatures (2.3, 2, and 1.8 K). The dimensionless parameter $h=\mu H/k_BT$ has been introduced with $\mu=9\mu_B$ the magnetic moment of a magnetic unit and μ_B the Bohr magneton. A quadratic dependence is observed at low fields, while a quasilinear variation is found for larger h values (typically above 0.2). Moreover, it should be mentioned that ν_{nor} versus h plots are clearly temperature dependent even after using normalized parameters. It is worth noting that these data on powder samples cannot be directly compared to the theory, as an average of the theoretical result should be first performed to account for the distribution of the magnetic field projections along the easy axis. This discussion will be developed in the following section.

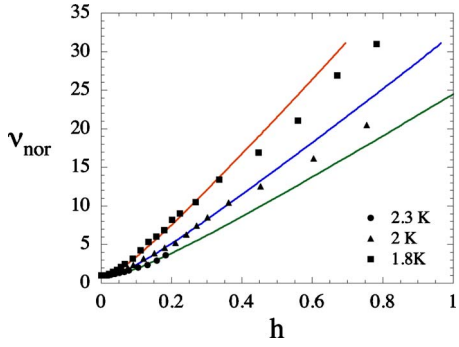

FIG. 12. (Color online) Normalized characteristic frequency deduced from ac data for the Mn/Fe chain on a powder sample: full dots, $T=2.3$ K; full triangles, $T=2$ K; full squares, $T=1.8$ K. The continuous lines give the fit discussed in Sec. IV.

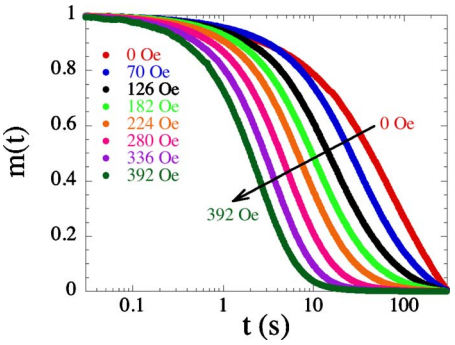

FIG. 13. (Color online) Time dependence of the magnetization (normalized between $t=0$ and $t=\infty$) obtained at $T=1.05$ K from the dc measurement on single crystal of the Mn/Fe chain when the field is applied in the easy direction.

To obtain data at lower temperatures, in the finite-size regime, we have also performed dc measurements on oriented single crystals using homemade micro-SQUID equipment as previously described.[34] In this experiment, a large negative magnetic field (−1.1 T) is first applied to saturate the magnetization. Then, the magnitude of the field is increased up to the chosen field value and the relaxation of the magnetization is deduced as a function of time. Figure 13 gives typical results obtained at 1.05 K for different values of the magnetic field. The relaxation time of the system is simply extracted from the normalized data, taking the value of the time when the normalized signal is equal to $1/e$. A large field dependence of this characteristic time is observed and can be directly compared with the theory. First, the critical regime at very low field can be analyzed through the expected quadratic dependence of the normalized frequency. As shown in Fig. 14(a), this behavior is indeed observed as a linear plot is obtained when this frequency is plotted as a function of h^2. The resulting slope gives a_i and therefore the effective chain length λ using the data shown in Fig. 8, i.e., $\lambda=20$ and 30 at 1.05 and 1.25 K, respectively. A less accurate set of data at 1.35 K gives $\lambda\approx35$ at this temperature. These values are reported in Fig. 10(a) (blue squares) to show the coherence with susceptibility data. The normalized frequency at 1.05 and 1.25 K is plotted in Fig. 14(b) as a function of $h\lambda$. A large field dependence of the relaxation frequency is found and will be further discussed in the following section.

C. Single-chain magnet behavior under magnetic field in the Mn/Ni chain

For this sample, ac measurements have been performed on both powder sample and single crystals. In the latter case, a Hall probe has been used in homemade equipment.[34] From ac data on a powder sample performed at two temperatures (3.8 and 4.4 K), the field dependence of the characteristic frequency has been obtained. After normalization of the characteristic frequency (ν_{nor}) and using the dimensionless h parameter with $\mu=6\mu_B$ (Fig. 15), a single master curve is observed. In contrast with the data obtained for the Mn/Fe chain, the field dependence for the Mn/Ni chain is very

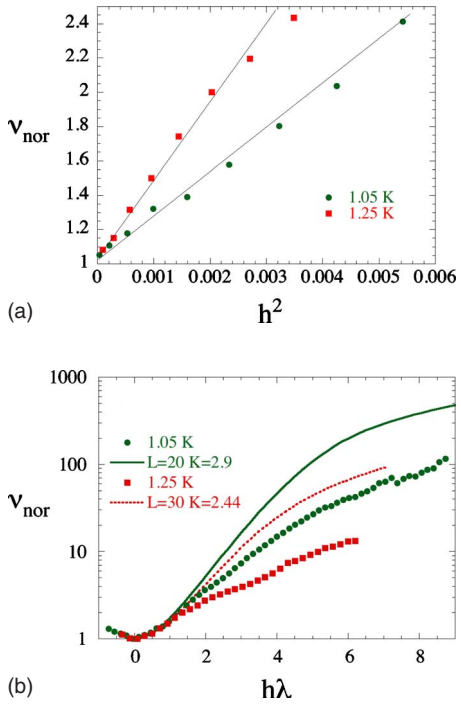

FIG. 14. (Color online) For the Mn/Fe chain: (a) Quadratic behavior obtained at low field: a linear plot is obtained plotting $\nu_{nor}(h^2)$. The deduced values of the effective length λ are 20 and 30 at 1.05 and 1.25 K, respectively. (b) Normalized relaxation frequency obtained from dc measurements on single crystals as a function of $h\lambda$: full dots, $T=1.05$ K; full squares, $T=1.25$ K. The continuous and dotted lines correspond to the numerical calculation for ($L=20$, $K=2.9$) and ($L=30$, $K=2.44$), respectively.

weak, i.e., the relaxation time remains large even when $h\lambda \gg 1$ [note that this regime is very quickly obtained in this system as λ reaches much higher values than the Mn/Fe chain as emphasized by Fig. 10(b)]. This distinctive behavior is confirmed by the data obtained at 5 K on single crystal (Fig. 16). In this figure, the amplitude of frequency variation is less than 3.5 between $H=0$ and the largest fields shown in the figure for which the magnetization is already almost saturated at equilibrium. This contrast between the dynamic properties of two chains will be analyzed in the following

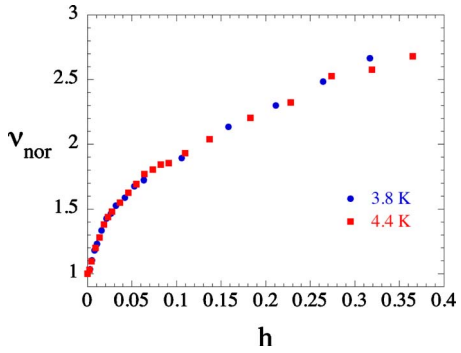

FIG. 15. (Color online) Normalized characteristic frequency deduced from ac susceptibility data on a powder sample for the Mn/Ni chain: full dots, $T=3.8$ K; full squares, $T=4.4$ K.

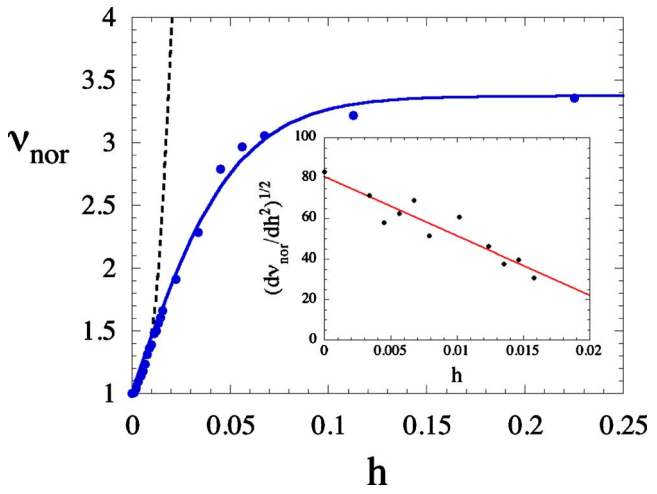

FIG. 16. (Color online) Normalized characteristic frequency deduced from dc measurements at 5 K on single crystal for the Mn/Ni chain when the field is applied in the easy direction. The dotted line gives the theoretical prediction for $L=80$, $K=2.8$ assuming a constant value of τ_0. Inset: The derivative of the normalized frequency relative to h^2 is shown to emphasize the extrapolation close to 80 for $h=0$. Continuous lines are guides for the eyes.

section. As in the previous case, the critical regime should also be discussed. Because of the large values of λ, this critical domain is restricted to very low fields (typically $h \ll 0.01$), and a quadratic behavior is not so easily seen in Fig. 16. For this reason and in order to highlight this regime, the plot of $(d\nu_{nor}/dh^2)^{1/2}$ as a function of h has been given in the inset of Fig. 16. It is worth noting that the extrapolation at zero field is, in fact, of the order of $\lambda \approx 80$ in coherence with Fig. 10(b).

IV. ANALYSIS OF THE DATA

A. Mn/Fe chain

In order to compare the ac results, performed on a powder sample, to the theory discussed in Sec. II, it is important to realize that the powder averaging effect has to be taken into account in the model (by assuming a random distribution of the easy axis among the powder sample that implies a distribution of the component of the magnetic field along the easy axis and therefore a distribution of the magnetic responses). The calculation of the resulting field dependence of the relaxation frequency for an infinite chain is given in Appendix D. The obtained results (continuous lines in Fig. 12) can then be compared with the experimental data that are essentially obtained in the exponential regime, i.e., above the crossover temperature induced by finite-size effects. As shown in Fig. 12, an excellent agreement is found both at very low field (in the critical regime) and at higher fields up to $h \approx 0.4$. The deduced values of $\lambda = e^{2K}$ are reported in Fig. 10(a) (red dots). As for dc data, they are in excellent agreement with the estimation of $\lambda(T)$ from susceptibility data (note that there is no adjustable parameter for this analysis). This result highlights that (i) the expected critical behavior is, in fact, ob-

served and (ii) an agreement with the theory is also preserved for field values up to he^{2K} of the order of 8–11. However, both at 1.8 and at 2 K, a significant departure between the theory and the experiment is found above $h \approx 0.4$ that will be discussed after analyzing further the dc data that are shown in Fig. 14. As these data are taken in the finite-size regime, the values of λ deduced from the analysis of the critical regime should be interpreted as a temperature dependent effective chain length of the system (see previous section). Then, these experimental results should be compared with the theoretical curves obtained for the same values of L (K is also known as J_I has been estimated from susceptibility data). These theoretical data are given in Fig. 14: the continuous line corresponds to $T=1.05$ K ($L=20$, $K=2.9$), while the dotted line is associated with $T=1.25$ K ($L=30$, $K=2.44$). As for the ac data, the agreement is only realized at low field and a significant departure between the experiment and the theory is found above $h\lambda \approx 1$. To understand this result, it should be realized that the theoretical curves are obtained assuming that τ_0 [introduced in Eq. (3)] is not field dependent. In reality, the characteristic time for a spin flip of a magnetic unit inside a domain wall is probably changing with H. The situation of this magnetic unit is, in fact, close, although not identical, to the one experienced by an isolated unit. In this latter case, the magnetic unit can be considered as a single molecule magnet (SMM) for which the field dependence of the relaxation time has been extensively studied. In fact, the characteristic time of a SMM is expected to increase as the magnetic field increases. In particular, a large effect is predicted when quantum effects are relevant for the relaxation process, and a quadratic dependence of the relaxation time is then predicted in a simple approach.[35] To estimate the field variation of τ_0, the ratio between the experimental points and the theoretical estimation of the SCM relaxation time has been made for $L=30$, $K=2.44$. The result is given in Fig. 17(a) and is, in fact, consistent with a quadratic field variation of τ_0. The continuous line gives the fit assuming a quadratic dependence: $\tau_0(h)/\tau_0(0)=1+(h/h_0)^2$, with $h_0=0.385$. This also implies $\tau_0(H)/\tau_0(0)=1+(H/H_0)^2$, with $H_0=244$ G.

A further analysis can be made comparing this result with the one obtained for isolated trinuclear motifs. In the case of the Mn/Fe chain, a sample presenting such quasi-isolated magnetic units, $(NEt_4)[Mn_2(salmen)_2(MeOH)_2Fe(CN)_6]$, has, in fact, been synthesized and studied for $H=0$.[5] For a deeper analysis, the field dependence of the relaxation time has been measured on a powder sample of this system. To compare with the chain data obtained on an oriented single crystal, an average of the previously deduced $\tau_0(h)$ [Fig. 17(a)] has been made using the technique described in Appendix D but taking χ_d constant (as the sample follows a Curie behavior with a field independent susceptibility at low field). Figure 17(b) shows that a good agreement is obtained between experience and theory that further reinforces our interpretation and thus the key role played by the field dependence of τ_0 to understand the relaxation of the magnetization under magnetic field in SCM systems.

B. Mn/Ni chain

Comparing with the Mn/Fe chain, the data for the Mn/Ni chain suggest an even stronger effect of the field dependence

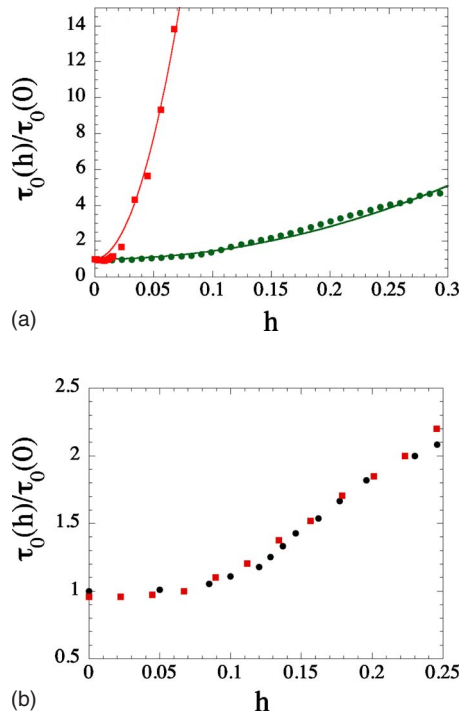

FIG. 17. (Color online) (a) Deduced field dependence of $\tau_0(h)/\tau_0(0)$ for the Mn/Fe chain (full dots) and the Mn/Ni chain (full squares), normalizing the single crystal data obtained, respectively, at 1.25 and 5 K to the theoretical result. The continuous lines give the fits to a quadratic dependence $[\tau_0(h)/\tau_0(0)=1+(h/h_0)^2]$, with $h_0=0.385$ and 0.139 for the Mn/Fe and Mn/Ni chains, respectively. (b) Comparison of the averaged result obtained from the data shown in (a) for the Mn/Fe chain (full dots) to the experimental data obtained at 1.8 K for $(NEt_4)[Mn_2(salmen)_2(MeOH)_2Fe(CN)_6]$ (full squares).

of τ_0, which, in this case, almost compensates the field dependence coming from the thermodynamics. As in the previous case, the field dependence of τ_0 can be obtained by dividing the experimental data shown in Fig. 16 by the thermodynamic theoretical result calculated for a constant τ_0 value. In agreement with the estimated values of J_I and L, we have taken $K=2.8$ and $L=80$ (dotted line in Fig. 16). The obtained result is also given in Fig. 17(a). Again, a quadratic field dependence is observed with a value of h_0 close to 0.14. This corresponds to $H_0=254$ G. Although similar values of H_0 are found, the effect on the experimental results is better discussed considering the reduced variable h. As shown in Fig. 17(a), a stronger dependence of $\tau_0(h)$ is then found for the Mn/Ni chain, which can explain a more drastic influence on the field dependence of the normalized characteristic frequency. For a deeper discussion about this dependence, it would be necessary to compare with the relaxation time of isolated Mn/Ni trinuclear units. Unfortunately, even if materials containing almost isolated Mn/Ni trinuclear units have been recently synthesized,[36] the presence of weak intermolecular magnetic interactions did not allow us to use them for the present discussion. However, it can be noted that Fig. 15 shows a universal behavior when the normalized frequency is plotted as a function of h. As the thermodynamic

contribution is a function of this reduced variable, this result suggests that it is also the case for τ_0. However, a quantitative theory accounting for the field dependence of τ_0 is still missing, and it is hard to comment further on this result. Moreover, ac experiments are only possible in a narrow window of temperatures (3.8 and 4.4 K in the present experiment) because of the exponential temperature dependence of the relaxation time. Therefore, the plot of the normalized frequency as a function of H for these two temperatures is not far from a single curve, and it is not easy to propose accurate conclusions about the field dependence of τ_0 at the present stage.

Finally, it should be noted that the obtained field dependences are qualitatively similar for the two chains (at 1.25 and 5 K for the Mn/Fe and Mn/Ni chains, respectively). This point strongly suggests a common origin for the field variation of τ_0, reminiscent of those observed in SMMs.[35] Therefore similar thermal and quantum effects that are well known to control the magnetization relaxation in SMMs might be also relevant to understand the field variation of τ_0 in SCM systems.

V. CONCLUDING REMARKS

To conclude, we like to summarize the main results obtained in this paper. The central problem discussed in our work concerns the dynamic properties of single-chain magnets. The underlying theoretical description relies on the one-dimensional Ising model and its critical properties at low temperature and low applied magnetic field. The expected critical slowing down has been extensively discussed theoretically often starting from the transition probabilities introduced in the pioneering work of Glauber. However, the experimental realization of the resulting singular behavior is not so easily obtained. A striking example is given by the study of biopolymers. Even in the most detailed studies of this research field, only the critical regime ($s \approx 1$) has been probed.[37] In the present work, we have shown that SCMs allow a more complete experimental study including the behavior at higher field and thus make possible a deeper comparison with the theory.

To achieve this goal, we have first reviewed the main theoretical approaches and proposed a comparison with our own numerical results on a finite Ising chain. In this same section, we have emphasized the universal behavior in the critical regime but also the need to consider a model able to describe the relaxation at higher fields. In this latter case, the field dependence of the kinetic coefficients is expected to play a crucial role. In coherence with the work of Schwarz, we have shown that the major role is played by τ_0 that gives for the Ising chain the relaxation time of a spin inside a domain wall. The field dependence of the relaxation time is then expected to result from the combination of thermodynamic arguments on the Ising model and from the field dependence of the kinetic coefficient k_F introduced in Sec. II. An equivalent presentation is to assume a field dependence of the characteristic time τ_0.

Experimentally, two SCM systems have been compared and discussed in the frame of the theoretical arguments given in Sec. II. In both cases, the observed critical regime is consistent with the theory. At higher fields, a large difference is found between the two studied chains. This effect has been attributed to the significant field dependence of τ_0 coming from the intrinsic slow relaxation of the Mn/Ni and Mn/Fe trinuclear units.

In summary, we have shown that the field dependence of the relaxation time of a single-chain magnet is the result of combined macroscopic (i.e., thermodynamic) and molecular arguments. The present study also illustrates the importance of probing both the temperature and field dependences for a deep analysis of the magnetization relaxation in single-chain magnets.

ACKNOWLEDGMENTS

We thank A. Vindigni for illuminating discussions concerning the theory. This work was supported by the University Bordeaux I and the Conseil Régional d'Aquitaine, the CREST project, Japan Science and Technology Agency (JST), and a Grant-in-Aid for Scientific Research on Priority Areas (Grant No. 17036054, "Chemistry of Coordination Space") from the Ministry of Education, Science, Sports, and Culture of Japan.

APPENDIX A: LOCAL-EQUILIBRIUM APPROXIMATION FOR THE INFINITE CHAIN

The kinetic equation for the average of a spin is, following Glauber,

$$\tau_0 \frac{d\langle \sigma_p \rangle}{dt} + \langle \sigma_p \rangle = C + \frac{\gamma}{2}[\langle \sigma_{p-1} \rangle + \langle \sigma_{p+1} \rangle] - \frac{\gamma C}{2}[\langle \sigma_{p-1}\sigma_p \rangle + \langle \sigma_p \sigma_{p+1} \rangle], \quad \text{(A1)}$$

where $C=\tanh(h)$ and $\gamma=\tanh(2K)$. In the case of an infinite chain, each average is independent of p and one obtains

$$\tau_0 \frac{dm}{dt} + (1-\gamma)m = C - \gamma C \Gamma_1, \quad \text{(A2)}$$

where $\Gamma_1=\langle \sigma_{p-1}\sigma_p \rangle$ is the first neighbor correlation function. To apply the local-equilibrium approximation, we should use the relation existing between m and the correlation function at thermal equilibrium. It reads[38]

$$\Gamma_1 = m^2 + (1-m^2)\frac{\cosh h - \sqrt{\sinh^2 h + e^{-4K}}}{\cosh h + \sqrt{\sinh^2 h + e^{-4K}}}, \quad \text{(A3)}$$

with

$$m = \frac{\sinh h}{\sqrt{\sinh^2 h + e^{-4K}}}. \quad \text{(A4)}$$

This implies

$$\Gamma_1 = 1 - \frac{2(1-m^2)}{\sqrt{m^2 + (1-m^2)e^{4K}} + 1}. \quad \text{(A5)}$$

If this relation is introduced in the above kinetic equation, one obtains a nonlinear equation describing the evolution of

$m(t)$. To describe the linear response of the chain (small departure from thermal equilibrium), this equation should be linearized. Introducing $\delta m(t)=m(t)-m_{eq}$, where m_{eq} is the value of m for the final equilibrium state, one obtains

$$\tau_0 \frac{d\delta m}{dt} + \left(1 - \gamma + \gamma C \left(\frac{d\Gamma_1}{dm}\right)_{eq}\right)\delta m = 0. \tag{A6}$$

A straightforward calculation gives

$$\left(\frac{d\Gamma_1}{dm}\right)_{eq} = 2C. \tag{A7}$$

This gives an exponential relaxation of the magnetization with the characteristic time:

$$\tau = \frac{\tau_0}{1 - \gamma + 2\gamma C^2}. \tag{A8}$$

At low temperature, this expression can be simplified:

$$\tau(C) = \frac{\tau(C=0)}{1 + e^{4K} C^2}. \tag{A9}$$

Then, the critical behavior is correctly reproduced at low field. Although the relaxation time is slightly underestimated when $C \to 1$, this simple expression remains close to the complete expression of τ described in Sec. II outside of the critical domain and can therefore be used to analyze the experimental data.

APPENDIX B: LOCAL-EQUILIBRIUM APPROXIMATION FOR A FINITE CHAIN

Matsubara *et al.*[8] have given exact results for a finite Ising chain (the spins are labeled from 1 to n). They obtain [Eq. (3.14) of these authors]

$$\langle \sigma_p \sigma_{p+1} \rangle_n = \frac{u + \langle \sigma_p \rangle_p \langle \sigma_{n-p} \rangle_{n-p}}{1 + u \langle \sigma_p \rangle_p \langle \sigma_{n-p} \rangle_{n-p}}, \tag{B1}$$

where $\langle \sigma_p \rangle_p$ is the average value of the end spin of a chain of size p and $u=\tanh K$. The same authors also give [Eq. (3.12)]:

$$\langle \sigma_p \rangle_n = \frac{C + u(\langle \sigma_{p-1} \rangle_{p-1} + \langle \sigma_{n-p} \rangle_{n-p}) + u^2 C \langle \sigma_{p-1} \rangle_{p-1} \langle \sigma_{n-p} \rangle_{n-p}}{1 + uC(\langle \sigma_{p-1} \rangle_{p-1} + \langle \sigma_{n-p} \rangle_{n-p}) + u^2 \langle \sigma_{p-1} \rangle_{p-1} \langle \sigma_{n-p} \rangle_{n-p}} \tag{B2a}$$

and

$$\langle \sigma_p \rangle_p = \frac{C + u \langle \sigma_{p-1} \rangle_{p-1}}{1 + uC \langle \sigma_{p-1} \rangle_{p-1}}. \tag{B2b}$$

This relation implies

$$\langle \sigma_p \rangle_n = \frac{\langle \sigma_p \rangle_p + u \langle \sigma_{n-p} \rangle_{n-p}}{1 + u \langle \sigma_p \rangle_p \langle \sigma_{n-p} \rangle_{n-p}} \tag{B3a}$$

and

$$\langle \sigma_{p+1} \rangle_n = \frac{\langle \sigma_{n-p} \rangle_{n-p} + u \langle \sigma_p \rangle_p}{1 + u \langle \sigma_p \rangle_p \langle \sigma_{n-p} \rangle_{n-p}}. \tag{B3b}$$

The next step is the linearization of Eqs. (B1), (B3a), and (B3b), to estimate $\delta\langle \sigma_p \sigma_{p+1} \rangle_n$ as a function of $\delta\langle \sigma_p \rangle_n$ and $\delta\langle \sigma_{p+1} \rangle_n$. A rather long but straightforward calculation gives

$$\delta\langle \sigma_p \sigma_{p+1} \rangle_n = A_{n,p} \delta\langle \sigma_p \rangle_n + B_{n,p} \delta\langle \sigma_{p+1} \rangle_n, \tag{B4}$$

with

$$A_{n,p} = \frac{\langle \sigma_{n-p} \rangle_{n-p,eq} - u \langle \sigma_p \rangle_{p,eq}}{1 - u \langle \sigma_p \rangle_{p,eq} \langle \sigma_{n-p} \rangle_{n-p,eq}} \tag{B5a}$$

and

$$B_{n,p} = \frac{\langle \sigma_p \rangle_{p,eq} - u \langle \sigma_{n-p} \rangle_{n-p,eq}}{1 - u \langle \sigma_p \rangle_{p,eq} \langle \sigma_{n-p} \rangle_{n-p,eq}}, \tag{B5b}$$

where the average values in these last two equations are taken at equilibrium.

To conclude this calculation, the explicit expression of the spin averages should be introduced in the above coefficients:

$$\langle \sigma_p \rangle_{p,eq} = C \frac{\lambda_+^p - \lambda_-^p}{\lambda_+^{p+1} - \lambda_-^{p+1} - u(\lambda_+^p - \lambda_-^p)}, \tag{B6}$$

with

$$\lambda_\pm = \frac{1+u}{2} \pm \sqrt{(1-u)^2 + 4uC^2}. \tag{B7}$$

Note that this expression is equivalent to Eq. (56) of Ref. 19.

APPENDIX C: RELAXATION OF A FINITE CHAIN IN PRESENCE OF AN APPLIED FIELD

We consider the relaxation of a finite chain composed of n identical Ising spins labeled from 1 to n. The corresponding Hamiltonian is similar to the one given by Eq. (2). As before, $u=\tanh K$, $\gamma=\tanh(2K)$ $(K>0)$, and $C=\tanh(h)$, where h is the dimensionless applied magnetic field.

The equation of motion for an interior spin is (in the following, the index n used in Appendix B is omitted)

$$\tau_0 \frac{d\langle \sigma_p \rangle}{dt} + \langle \sigma_p \rangle = C + \frac{\gamma}{2}[\langle \sigma_{p-1} \rangle + \langle \sigma_{p+1} \rangle] - \frac{\gamma C}{2}[\langle \sigma_{p-1} \sigma_p \rangle + \langle \sigma_p \sigma_{p+1} \rangle]. \tag{C1}$$

At the end on the segment, we have

$$\tau_0 \frac{d\langle \sigma_1 \rangle}{dt} + \langle \sigma_1 \rangle = C + u \langle \sigma_2 \rangle - Cu \langle \sigma_1 \sigma_2 \rangle \tag{C2a}$$

and

$$\tau_0 \frac{d\langle \sigma_n \rangle}{dt} + \langle \sigma_n \rangle = C + u \langle \sigma_{n-1} \rangle - Cu \langle \sigma_{n-1} \sigma_n \rangle. \tag{C2b}$$

Linearization of the above equations gives (introducing $\delta\langle \sigma_p \rangle = \langle \sigma_p \rangle - \langle \sigma_p \rangle_{eq}$, where $\langle \sigma_p \rangle_{eq}$ is the equilibrium value of the considered spin, a similar notation being used for the correlation functions)

$$\tau_0 \frac{d\delta\langle\sigma_p\rangle}{dt} + \delta\langle\sigma_p\rangle = \frac{\gamma}{2}[\delta\langle\sigma_{p-1}\rangle + \delta\langle\sigma_{p+1}\rangle] - \frac{\gamma C}{2}[\delta\langle\sigma_{p-1}\sigma_p\rangle + \delta\langle\sigma_p\sigma_{p+1}\rangle], \tag{C3}$$

with

$$\tau_0 \frac{d\delta\langle\sigma_1\rangle}{dt} + \delta\langle\sigma_1\rangle = u\delta\langle\sigma_2\rangle - Cu\delta\langle\sigma_1\sigma_2\rangle \tag{C4a}$$

and

$$\tau_0 \frac{d\delta\langle\sigma_n\rangle}{dt} + \delta\langle\sigma_n\rangle = u\delta\langle\sigma_{n-1}\rangle - Cu\delta\langle\sigma_{n-1}\sigma_n\rangle. \tag{C4b}$$

The local-equilibrium approximation will be used to relate the variations of correlation functions to the spin variables. We have shown in Appendix B that

$$\delta\langle\sigma_p\sigma_{p+1}\rangle = A_{n,p}\delta\langle\sigma_p\rangle + B_{n,p}\delta\langle\sigma_{p+1}\rangle, \tag{C5}$$

where $A_{n,p}$ and $B_{n,p}$ are given by Eqs. (B5a) and (B5b). Then, Eqs. (A4) and (A5) become

$$\tau_0 \frac{d\delta\langle\sigma_p\rangle}{dt} + \delta\langle\sigma_p\rangle\left(1 + \frac{\gamma C}{2}(B_{n,p-1} + B_{n,p})\right) = \frac{\gamma}{2}(1 - CA_{n,p-1})\delta\langle\sigma_{p-1}\rangle + \frac{\gamma}{2}(1 - CA_{n,p})\delta\langle\sigma_{p+1}\rangle, \tag{C6}$$

with

$$\tau_0 \frac{d\delta\langle\sigma_1\rangle}{dt} + (1 + uCA_{n,1})\delta\langle\sigma_1\rangle = u(1 - CB_{n,1})\delta\langle\sigma_2\rangle \tag{C7a}$$

and

$$\tau_0 \frac{d\delta\langle\sigma_n\rangle}{dt} + (1 + uCB_{n,n-1})\delta\langle\sigma_n\rangle = u(1 - CA_{n,n-1})\delta\langle\sigma_{n-1}\rangle. \tag{C7b}$$

These last two equations are consistent with symmetric boundary conditions as $B_{n,n-1}=A_{n,1}$ and $A_{n,n-1}=B_{n,1}$. We obtain a set of linear equations which can be written in a compact form

$$\tau_0 \frac{d\Sigma}{dt} = -M\Sigma, \tag{C8}$$

where Σ is a vector with n components: $\delta\langle\sigma_p\rangle$. Numerically, the eigenvalues and the corresponding eigenvectors can be deduced. Considering a single-time approximation, the relaxation time is readily obtained from the estimation of the smallest eigenvalue $\lambda_{\min}$ of M:

$$\frac{\tau_0}{\tau} = \lambda_{\min}. \tag{C9}$$

However, the different eigenvalues and eigenvectors can also be compared to discuss the validity of the single-time approximation. This discussion is presented in Sec. II C.

APPENDIX D: RELAXATION OF A POWDER SAMPLE

Let us assume that the relaxation of a single crystal follows the Debye model (single-time approximation). Then, the average ac complex susceptibility for a powder reads

$$\langle\chi\rangle = \int_0^1 \chi_d \frac{u^2 du}{1 + i\omega\tau}, \tag{D1}$$

where $u=\cos\theta$, θ being the angle between the applied field and the easy axis of a given crystal inside the powder sample. The effective projection of the field seen by this crystal is $H=H_a\cos\theta$, and $\chi_d(H)$ is the corresponding differential susceptibility and τ is the relaxation time that also depends on H. H_a is the applied field.

Experimentally, the maximum of the imaginary part of the susceptibility is measured, and then we deduce from Eq. (D1)

$$\langle\chi''\rangle = \int_0^1 \chi_d \frac{\omega\tau u^2 du}{1 + \omega^2\tau^2}. \tag{D2}$$

Let us now specifically discuss the case of the infinite chain. The normalized differential susceptibility reads

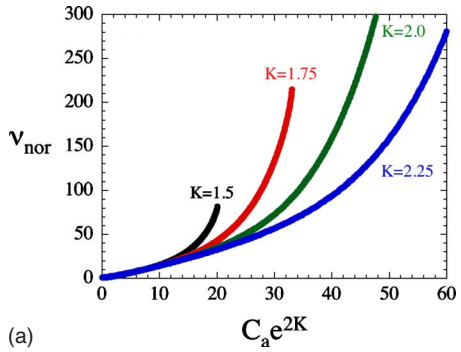

(a)

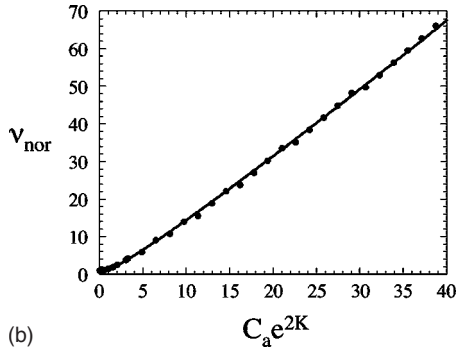

(b)

FIG. 18. (Color online) (a) Calculated normalized relaxation frequency for a powder sample in the infinite chain regime for different values of K. (b) Zoom on the low field regime where a single curve is obtained as a function of $C_a e^{2K}$ [this curve is still valid up to $C_a e^{2K}=40$ for the largest value of K shown in (a)]. The continuous line gives the empirical fit with $\nu_{nor} = 2\sqrt{1+0.406(C_a e^{2K})^{2.16}} - 1$.

$$\chi_d = \frac{\partial m}{\partial h} = \frac{e^{-4K}\cosh(h)}{(\sinh^2(h)+e^{-4K})^{3/2}} = \frac{e^{2K}(1-C^2)}{(1+bC^2)^{3/2}}, \quad \text{(D3)}$$

with

$$b = e^{4K} - 1 = \frac{2\gamma}{1-\gamma}$$

and $C=\tanh(h_a u)$. Considering $1/\tau(C)=[1/\tau(C=0)]\nu_{nor}(C)$, $x=\tau(C=0)\omega$, and $C_a=\tanh(h_a)$, we obtain

$$\langle \chi'' \rangle = \frac{e^{2K}x}{{h_0}^3}\int_0^{C_a} \frac{[\arctan h(C)]^2}{(1+bC^2)^{3/2}} \frac{\nu_{nor}(C)dC}{({\nu_{nor}}^2(C)+x^2)}. \quad \text{(D4)}$$

Then, the maximum of $\langle \chi'' \rangle$ is obtained by solving

$$\int_0^{C_a} \frac{\nu_{nor}(C)[\arctan h(C)]^2}{(1+bC^2)^{3/2}} \frac{[{\nu_{nor}}^2(C)-x^2]}{[{\nu_{nor}}^2(C)+x^2]^2} dC = 0. \quad \text{(D5)}$$

This gives the value of x at the maximum as a function of C_a. This x value can be identified with the normalized frequency obtained experimentally from a powder sample at the maximum of the imaginary part of the susceptibility.

We have first deduced the solution of Eq. (D5) numerically using the relaxation time given by Eq. (9) with the Glauber kinetic coefficients [Eq. (7)]. Figure 18(a) gives the obtained normalized frequency for different values of K as a function of $C_a \exp(2K)$. A single curve is obtained for small values of C_a, i.e., when the normalized frequency of a single crystal is a function of the reduced variable $C_a \exp(2K)$. This curve is given in Fig. 18(b). The continuous line is an empirical fit with $\nu_{nor}=2\sqrt{1+0.406(C_a e^{2K})^{2.16}}-1$. At higher field, the result depends on K as expected from the general expression given by Eq. (9).

The existence of a universal behavior at small field and low temperature is a consequence of Eq. (D5). In this limit, we have $b \approx e^{4K}$ and $\nu_{nor}(C) \approx 1+e^{4K}h^2$. Then, Eq. (D5) can be simplified into

$$\int_0^{z_a} \frac{z^2}{(1+z^2)^{1/2}} \frac{(z^2-x^2)}{(z^2+x^2)^2} dz = 0, \quad \text{(D6)}$$

where $z=e^{2K}h$ and $z_a=e^{2K}h_a$.

From Eq. (D6), it is clear that the deduced value of x is a function of the reduced variable z_a. Experimentally, data are only obtained in this low field regime where the comparison with the theory is simpler.

Finally, it should be noted that an approximate expression of the solution of Eq. (D6) can be obtained when $e^{2K}h_a \ll 1$ as

$$x = 1 + \frac{3}{5}e^{4K}h_a^2. \quad \text{(D7)}$$

This means that our analysis predicts a quadratic dependence of the normalized frequency of a powder sample for very small values of the applied field. The resulting curvature gives an estimation of $\lambda(T)=e^{2K}$ using Eq. (D7). At higher fields, Fig. 18(b) shows that a quasilinear behavior is then predicted.

[1] A. Caneschi, D. Gatteschi, N. Latioti, C. Sangrogorio, R. Sessoli, G. Venturi, A. Vindigni, A. Rettori, M. G. Pini, and M. A. Novak, Angew. Chem., Int. Ed. **40**, 1760 (2001).

[2] For a recent review, see C. Coulon, H. Miyasaka, and R. Clérac, Struct. Bonding (Berlin) **122**, 163 (2006).

[3] R. Clérac, H. Miyasaka, M. Yamashita, and C. Coulon, J. Am. Chem. Soc. **124**, 128837 (2002); H. Miyasaka, R. Clérac, K. Mizushima, K. Sugiura, M. Yamashita, W. Wernsdorfer, and C. Coulon, Inorg. Chem. **42**, 8203 (2003); A. Saitoh, H. Miyasaka, M. Yamashita, R. Clérac, J. Mater. Chem. **17**, 2002 (2007).

[4] C. Coulon, R. Clérac, L. Lecren, W. Wernsdorfer, and H. Miyasaka, Phys. Rev. B **69**, 132408 (2004).

[5] M. Ferbinteanu, H. Miyasaka, W. Wernsdorfer, K. Nakata, K. Sugiura, M. Yamashita, C. Coulon, and R. Clérac, J. Am. Chem. Soc. **127**, 3090 (2005).

[6] W. Wernsdorfer, R. Clérac, C. Coulon, L. Lecren, and H. Miyasaka, Phys. Rev. Lett. **95**, 237203 (2005).

[7] See, for example, C. J. Thompson, in *Phase Transitions and Critical Phenomena*, edited by C. Domb and M. S. Green (Academic, London, 1972), Vol. 1, p. 177.

[8] F. Matsubara, K. Yoshimura, and S. Katsura, Can. J. Phys. **51**, 1053 (1973).

[9] R. J. Glauber, J. Math. Phys. **4**, 294 (1963); see also M. Suzuki and R. Kubo, J. Phys. Soc. Jpn. **24**, 51 (1968).

[10] R. Cordery, S. Sarker, and J. Tobochnik, Phys. Rev. B **24**, 5402 (1981).

[11] The exact expressions for the one-dimensional Ising model valid at any temperature are $\xi=-1/\ln(\tanh K)$ and $\tau/\tau_0=1/(1-\tanh 2K)$.

[12] The dynamical exponent z is defined by $\tau \propto \xi^z$. See, for example, F. Haake and K. Thol, Z. Phys. B: Condens. Matter **40**, 219 (1980).

[13] L. Bogani, A. Caneschi, M. E. Fedi, D. Gatteschi, M. Massi, M. A. Novak, M. G. Pini, A. Rettori, R. Sessoli, and A. Vindigni, Phys. Rev. Lett. **92**, 207204 (2004).

[14] J. Kamphorst Leal da Silva, A. G. Moreira, M. Silverio Soares, and F. C. Sa Barreto, Phys. Rev. E **52**, 4527 (1995).

[15] J. H. Luscombe, M. Luban, and J. P. Reynolds, Phys. Rev. E **53**, 5852 (1996).

[16] G. Schwarz, J. Mol. Biol. **11**, 64 (1965).

[17] A. C. Pipkin and J. H. Gibbs, Biopolymers **4**, 3 (1966).

[18] M. E. Craig and D. M. Crothers, Biopolymers **6**, 385 (1968).

[19] G. Schwarz, Biopolymers **6**, 873 (1968).

[20] G. Schwarz, Rev. Mod. Phys. **40**, 206 (1968).

[21] G. Schwarz, J. Theor. Biol. **36**, 569 (1972).

[22] M. Schwarz, Jr. and D. Poland, J. Chem. Phys. **65**, 2620 (1976).

[23] A. Baumgartner and K. Binder, J. Chem. Phys. **70**, 429 (1979).

[24] A. Baumgartner and K. Binder, J. Stat. Phys. **18**, 423 (1978).

[25] Note that the empirical expression $1/\tau=2(\sinh^2 h+\sigma)/[\tau_0 \cosh(2h)]$ gives essentially the same field dependence

as Eq. (9) at low temperature when the Glauber kinetic parameters [Eq. (7)] are introduced.
[26] K. Kawasaki and T. Yamada, Prog. Theor. Phys. **39**, 1 (1968).
[27] H. W. Huang, Phys. Rev. A **8**, 2553 (1973).
[28] H. J. Hilhorst, Physica A **79**, 171 (1975).
[29] T. Tanaka, K. Soda, and A. Wada, J. Chem. Phys. **58**, 5707 (1973); T. Tanaka, A. Wada, and M. Suzuki, *ibid.* **59**, 3799 (1973).
[30] For example, taking $\exp(2K)=70$, the difference is at most of the order of 10%.
[31] D. Poland and H. A. Scheraga, J. Chem. Phys. **45**, 2071 (1966).
[32] http://www.scilab.org
[33] Note that the Schwarz model implies $\tau_L=\tau_\infty g(x)$, where $g(x)=1-(1-e^{-x})/x$ is the normalized magnetic susceptibility of a finite chain of size L ($x=L/\xi$). In practice, the functions $f(x)$ and $g(x)$ are very close to each other, in particular, for small values of x where finite-size effects are important.
[34] W. Wernsdorfer, Adv. Chem. Phys. **118**, 99 (2001).
[35] For a recent review, see, for example, I. Tupitsyn and B. Barbara, in *Magnetism: Molecules to Materials III, Nanosized Magnetic Materials*, edited by J. S. Miller and M. Drillon (Wiley-VCH, Weinheim, 2002), Vol. 3, p. 109.
[36] H. Miyasaka, T. Nezu, K. Sugimoto, K. Sugiura, M. Yamashita, and R. Clérac, Chem.-Eur. J. **11**, 1592 (2005).
[37] See, for example, Y. Tsuji, T. Yasunaga, T. Sano, and H. Ushio, J. Am. Chem. Soc. **98**, 813 (1976), and references therein.
[38] J. S. Marsh, Phys. Rev. **145**, 251 (1966).